Received: 20 August 2021 | Revised: 21 March 2022 | Accepted: 15 April 2022 | Published on: 24 May 2022

DOI: 10.1002/gamm.202200010

ORIGINAL PAPER

On the determination of thermal boundary conditions for parameter identifications of thermo-mechanically coupled material models

Lars Rose[1] | **Andreas Menzel**[1,2]

[1]Institute of Mechanics, TU Dortmund, Dortmund, Germany

[2]Division of Solid Mechanics, Lund University, Lund, Sweden

Correspondence
Lars Rose, Institute of Mechanics, TU Dortmund, Leonhard-Euler-Str. 5, D-44227 Dortmund, Germany. Email: lars.rose@tu-dortmund.de

Funding information
None reported.

Abstract

Identifiability and sensitivity of thermal boundary coefficients identified alongside thermal material parameters by means of full field measurements during a simple tension test are shown empirically using a simple tension test with self heating as a proof of concept. The identification is started for 10 different initial guesses, all of which converge toward the same optimum. The solution appears to be locally unique and parameters therefore independent, but a comparison against a reference solution indicates high correlation between three model parameters and the prescribed external temperatures required to model heat exchange with either air or clamping jaws. This sensitivity is further analyzed by rerunning the identification with different prescribed external temperatures and by comparing the obtained optimal parameter values. Although the model parameters are independent, optimal values for heat conduction and the heat transfer coefficients are highly correlated as well as sensitive with respect to a change, respectively, measurement error of the external temperatures. A precise fit on the basis of a simple tension test therefore requires precise measurements and a suitable material model which is able to accurately predict dissipated energy.

KEYWORDS

conduction, convection, coupled problem, inverse problem

1 | INTRODUCTION

The identification of suitable thermal boundary conditions is vital for any temperature related analysis, be it either a direct or inverse problem which is considered. In common engineering applications, boundary conditions of Robin-type often best describe the heat exchange between the body under consideration and its environment. This special kind of thermal boundary condition usually postulates a heat exchange along Newton's law of cooling which requires the temperature of the surrounding medium and a film or heat transfer coefficient. Obtaining the first parameter, that is, the temperature of the surrounding medium, is usually done by a simple measurement (assuming that this temperature is indeed constant over time). The definition of a suitable heat transfer coefficient, on the other hand, is usually not as simple since its value

may depend on material pairing, contact pressure or fluid velocity, general geometry as well as on surface roughness, see [11, Chapter 6]. Precise values for the heat exchange coefficients are therefore difficult to obtain from literature and must in general be identified for each type of boundary value problem.

Methods for such an inverse analysis date back as far as the 70s, see, for example, [5]. The method presented in that work minimizes the difference between experimental and computed data along certain grid points by using finite differences. Thereafter and with growing computational capability, methods for two-dimensional problems were derived. In [3], the identification of a time and space dependent heat transfer coefficient is demonstrated by means of a spherical body with symmetric temperature field. Moreover, [6] analyzes the heat exchange of an insulated, two-dimensional plate by using the boundary element method. At some point the terms inverse heat transfer coefficient problem (IHTCP) and inverse heat conduction problem (IHCP) were introduced and associated with the determination of film or heat transfer coefficients by means of inverse problems. Nowadays, the identification of heat transfer coefficients for three-dimensional boundary value problems poses no further computational problem and makes use of common solution methods for the underlying differential equations such as the finite volume method, see, for example, [7], or the finite element method, see, for example, [8]. However, all methods mentioned above require at least a subset of the classic thermal material parameters to be known, which especially includes the thermal conductivity of the body under consideration. These material parameters are usually identified by means of highly specialized experiments, for example, by using a guarded hot plate [9] or laser flashes, see, for example, [1,13]. For the inverse analysis of these experiments, either isothermal or adiabatic boundary conditions are applied, so that a heat transfer coefficient is not required and therefore neither needs to be estimated nor identified.

In contrast to the purely thermal investigations mentioned above, the method proposed in [12] and extended as well as successfully applied to experimental data in [14], aims at the identification of mechanical and thermal material parameters by means of a single experiment, for example, a simple tension test. Since common testing devices usually cannot guarantee isothermal or adiabatic bounds, heat transfer coefficients are required. Assumptions regarding these coefficients can be made for certain cases but they are unknown in general. This leads to the questions of identifiability and sensitivity of the thermal boundary coefficients alongside the actual thermal material parameters. To be more precise, related fundamental questions are

- Is a locally unique fit of thermal material parameters and boundary coefficients possible on the basis of full field temperature measurements?
- How sensitive are the resulting parameter values with respect to the (measured) boundary temperatures required for Newton's law of cooling?

This contribution therefore aims at answering the questions above in this proof of concept and considers the basics of parameter identification—that is, general framework, interpolation, choice of objective function, and so forth, as well as the identification of mechanical or thermal material parameters (without boundary coefficients) on the basis of a simple tension test—to be state of the art. These aspects are therefore not addressed in detail as this work proceeds. Readers unfamiliar with these topics are kindly referred to, for example, [14] and references cited therein, where more details and background is provided and on which the current work is based.

The article at hand is structured as follows. At first, the experimental setup as well as the experimental data used for the identification is presented in Section 2. Afterwards, the remaining input for the inverse problem (material model and boundary value problem) is summarized in the first part of Section 3. Before the identifiability of thermal material parameters alongside thermal boundary coefficients is analyzed in the same section, however, the objective function, the mechanical material parameters used for the simulation as well as a reference solution obtained with prescribed boundary coefficients are introduced. With this information at hand, a grid search optimization is performed in Section 3.6 to study the identifiability and uniqueness of the obtained solution within a certain area in parameter space. Alternative and mathematically more stringent methods, for example, employing the Hessian of the objective function, are commented on, and the resulting parameter values as well as the material response of the simulation based thereon are compared against the reference solution. Thus, the improvement in precision using optimized boundary conditions is shown in terms of both relative and absolute error improvement. The sensitivity of the optimum with respect to the prescribed temperature values of the external media required for Newton's law of cooling is analyzed thereafter by rerunning the identification several times with different, prescribed external temperatures. Finally, the possibility of identifying only a subset of thermal material parameters and boundary coefficients is explored in Section 3.7, prescribing the values of those thermal material parameters which can be identified by means of specialized experiments and are usually available

in literature, that is, thermal expansion, heat capacity, and thermal conduction. The obtained result is again compared against the fully optimized material response. The article closes with a conclusion in Section 4.

2 | EXPERIMENTS

The experimental data of a simple tension test used for the parameter identifications later on is presented in this section. The general setup is shown first, including a short paragraph on the handling of external infra-red radiation. The section closes with a brief analysis of the obtained experimental data. It is worth mentioning that only data of a single experiment is used, since this work is concerned with a general proof of concept, that is, a proof of identifiability. The use of data stemming from further repetitions of the same experiment would, however, not change the experiment intrinsic property of identifiability regarding specific (sub) sets of model parameters. If the result of an identification is to be used for predictive simulations, further data should of course be considered to account for random measurement errors.

2.1 | Experimental setup

Experiments were performed using an electro-mechanical tensile machine from Walter&Bai and classic dogbone shaped specimen made of the aluminum alloy AW6016, see Figure 1. Displacement and temperature field data were obtained by using a DIC system from GOM (resolution of 4 MPx) and a thermography system from InfraTec (ImageIR 8320hp, detected wavelengths between 2.0 and 5.7 µm). A speckle pattern was applied to one side and a black coating with a known emission coefficient of 0.98 to the other side of the specimen. An example of the speckle pattern quality can be found in [15]. The two measuring systems were then placed on either side of the specimen and started simultaneously by means of a trigger signal, as depicted in Figure 2.

A glass plate is included in the experimental setup, dividing the specimen from the DIC system which emits a significant amount of radiation due to the (comparatively) high temperature of the DIC device itself. This external and inhomogeneous infra-red radiation leads to an inhomogeneous temperature distribution in the specimen, even in a steady state prior to loading. Although the glass plate may not reduce this radiation to zero, it nevertheless serves as a filter for electromagnetic waves, since its transmission coefficient is high for waves in the visible, but low for waves in the infra-red spectrum. Thus, the glass plate reduces the spotlight-like radiation of the DIC device. It may heat up itself while doing so but the glass emits a more homogeneously distributed radiation due to its own conductivity. The reduced and homogenized residual emission can now be neglected for small temperature changes of the specimen if only the changes in temperatures are considered, assuming that the influence of the external heat sources on the specimen's temperature is not a function of this temperature itself, at least for the small temperature changes considered in this work. Conventional paper screens are used to protect the specimen from external radiation in directions where visibility is of no concern.

2.2 | Experimental data

The specimen was loaded for 140 s with a cross-head speed of 0.14 mm/s up to a total of 19.6 mm. Afterwards, the specimen was unloaded under displacement-controlled conditions until a reaction force of 0 N was reached. The specimen was

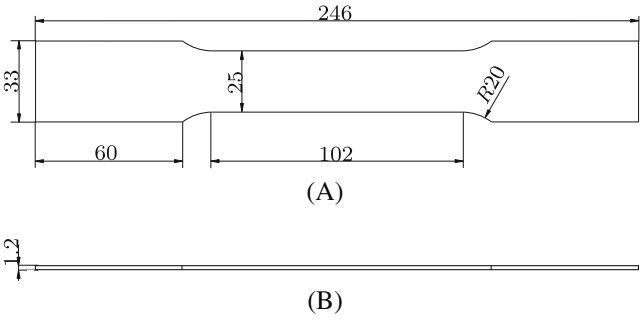

FIGURE 1 Dogbone specimen for tensile testing. (A) Technical drawing—top view and (B) technical drawing—front view. Reprinted from [14], with permission from Elsevier.

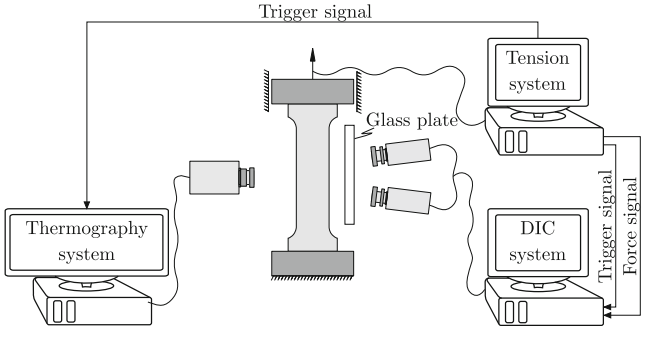

FIGURE 2 Setup of measuring devices for simple tension test. Reprinted from [14], with permission from Elsevier.

observed for 410 more seconds afterwards. Load was only applied after the specimen reached a steady state in terms of temperature. It is worth mentioning that both temperatures were tracked throughout the entire procedure by means of thermocouples and no significant changes were detected, see Figure 3. It is therefore straightforward to assume that the temperature of air and clamping jaws are constant for the experiment at hand as well, see Table 1.

Although full field information was obtained and used for the identification process later on, data with respect to the center point of the specimen is given in Figure 4 for the sake of interpretation and representation over time. Thereby, $P_{||}$ denotes the Piola stress in tensile direction and $F_{||}$ the related contribution of the deformation gradient. It can be seen that the alloy under consideration undergoes elastic cooling before plasticity induced heat sources lead to a temperature rise $\Delta\theta$ of approximately 3.5 K. During unloading, the inverse Gough–Joule effect leads to additional heating, followed by the cooling down of the specimen to room temperature. It is worth mentioning, that the temperature is inhomogeneously distributed almost right from the start of the experiment due to the specific boundary conditions at hand, that is, the clamping jaws at either end of the specimen, see Figure 5.

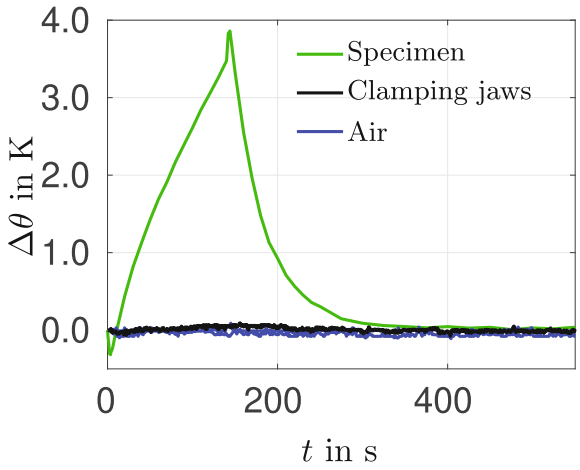

FIGURE 3 Temperature of specimen (center point) and environment during the experiment. Environmental temperatures were measured using thermocouples.

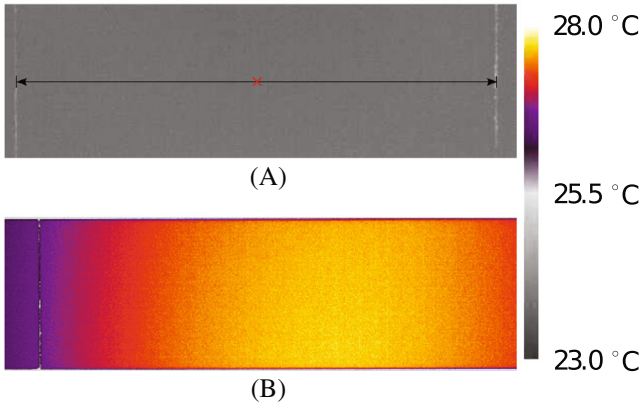

FIGURE 5 Temperature field of specimen during the experiment. Length of black line is 76 mm. Center of specimen is marked by red cross. (A) Initial temperature distribution and (B) temperature field directly after unloading s

TABLE 1 Measured temperatures of the surrounding media prior to loading

Clamping jaws (°C)	Air (°C)
23.55	24.25

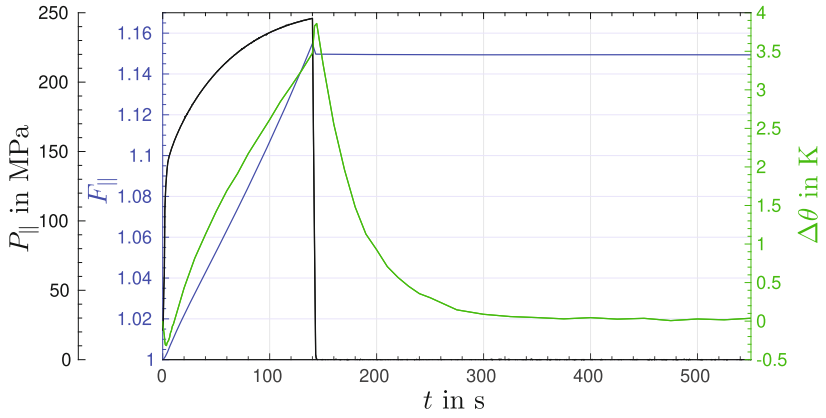

FIGURE 4 Experimental data at center point of specimen over time

3 | PARAMETER IDENTIFICATION

The results of several parameter identifications are shown within this section, whereas the main focus lies on the identifiability of heat conduction and heat convection coefficients alongside the unknown thermal material parameters. First, however, the underlying material model is briefly described and main equations referring to the thermal problem are shown. Afterwards, the boundary value problem as well as the objective function are defined before introducing the optimal mechanical parameters for the underlying problem as well as a reference solution for the optimal thermal material parameters. The actual identifiability of the whole set of unknown model parameters is shown afterwards by using a grid search approach. This is followed by a sensitivity analysis of the optimal parameter values with respect to the external, prescribed temperatures. Finally, the possibility to optimize only a subset of the thermal model parameters is explored and the result is compared against the fully optimized parameter set. All identifications are performed by using a Nelder–Mead-simplex with restart option and the successive identification scheme as proposed in [14].

3.1 | Material model

The chosen model is fully thermo-mechanically coupled featuring the Hill48 yield surface, an isotropic, saturation type hardening with non-associated evolution equations, surface elements for heat exchange with the environment as well as a material parameter to scale the predicted dissipation independent of mechanical material parameters within a thermodynamically consistent framework. The model is valid for large deformations and uses the classic multiplicative split of the deformation gradient into an elastic and plastic contribution. The capability of this model to represent the main aspects of the aluminum alloy under consideration was already demonstrated in [15], where a detailed derivation of model equations can also be found. Hence, only three equations are highlighted within this section, since the main focus of the work at hand lies on the general identifiability of thermal parameters and thermal boundary conditions and less on model specific properties. A brief summary of all relevant model equations and a specification of the underlying free Helmholtz energy ψ can be found in Appendix A.

The strong form of the balance of energy

$$c_0\ \dot{\theta} = \rho_0\ r - \nabla_{\boldsymbol{X}} \cdot \boldsymbol{Q}\left(\bullet\ ;\ \kappa_{\text{therm}}\right) + \mathcal{D}^{\text{mech}} + \theta\ \frac{\partial^2 \psi\left(\bullet\ ;\ \alpha_{\text{exp}}\right)}{\partial \boldsymbol{F}^{\text{el}}\ \partial \theta}\ :\ \dot{\boldsymbol{F}}^{\text{el}} \tag{1}$$

is chosen to introduce the classic set of thermal material parameters. These are the constant referential heat capacity $c_0 = -\theta\ \frac{\partial \psi}{\partial \theta^2}\ \frac{\partial \psi}{\partial \theta}$, the thermal heat conduction κ_{therm} as well as the thermal expansion coefficient α_{exp}. Here, $\dot{\theta}$ denotes the rate of temperature, ρ_0 is the referential mass density and r corresponds to the volumetric heat source. The referential divergence of the referential heat flux and the elastic part of the deformation gradient are represented by $\nabla_{\boldsymbol{X}} \cdot \boldsymbol{Q}$ and $\boldsymbol{F}^{\text{el}}$, respectively. The model-specific mechanical dissipation

$$\mathcal{D}^{\text{mech}} = \lambda_{\text{pm}}\ \left[b\ h\ \alpha^2 + [1-\beta]\, b\ M_{y_0} \alpha + \beta\ M_{y_0}\right] \tag{2}$$

depends on the mechanical material parameters b, h and M_{y_0} governing the rate, the saturation and the initial yield limit of the plastic hardening. It is a function of the current state of plasticity due to the plastic multiplier λ_{pm} and the internal hardening variable α. Furthermore, the material parameter β allows an additional adjustment of the predicted dissipation independent of the mechanical material behavior, see [2,15] and Appendix A for further details. Lastly, the thermal boundary coefficients are introduced by means of the governing equation for the employed surface elements. Heat flow over the boundary of the body under consideration is modeled using Newton's law of cooling, that is,

$$q_0 = \boldsymbol{n} \cdot \boldsymbol{q} = -\alpha_{\text{con}}\ \left[\theta^{\text{M}} - \theta\right], \tag{3}$$

with the heat conduction, or heat convection coefficient α_{con} and the temperature of the surrounding medium θ^{M}.

3.1.1 | General identifiability of the heat equation

The heat equation, which is based on the balance of energy, is the main equation on which the identification of thermal model parameters is based. Depending on the boundary value problem considered, it can take slightly different forms, for example,

$$c_0\ \dot{\theta} = -\nabla_{\boldsymbol{X}} \cdot \boldsymbol{Q}\left(\bullet\ ;\ \kappa_{\text{therm}}\right) \qquad \wedge \qquad \boldsymbol{n} \cdot \boldsymbol{q} = -\alpha_{\text{con}}\ \left[\theta^{\text{M}} - \theta\right] \tag{4}$$

for a body with transient change in temperatures and subject to convection at its boundary. Due to the specific definition of the heat flux, which is linear in the model parameter κ_{therm}, the model parameters of all addends can be factorized. Equation (4) can therefore be rewritten as

$$c_0\ \dot{\theta} = -\kappa_{\text{therm}}\ \nabla_{\boldsymbol{X}} \cdot \overline{\boldsymbol{Q}} \qquad \wedge \qquad \kappa_{\text{therm}}\ \boldsymbol{n} \cdot \overline{\boldsymbol{q}} = -\alpha_{\text{con}}\ \left[\theta^{\text{M}} - \theta\right], \tag{5}$$

$$\Leftrightarrow \quad \dot{\theta} = -\frac{\kappa_{\text{therm}}}{c_0}\ \nabla_{\boldsymbol{X}} \cdot \overline{\boldsymbol{Q}} \qquad \wedge \qquad \frac{\kappa_{\text{therm}}}{c_0}\ \boldsymbol{n} \cdot \boldsymbol{q} = -\frac{\alpha_{\text{con}}}{c_0}\ \left[\theta^{\text{M}} - \theta\right], \tag{6}$$

showing that only a subset of all parameters can be uniquely identified. This is true, as long as the main set of equations consists only of addends with different model parameters which can be factorized. Hence, adding different features to the experiment, for example, the effect of plastic heat sources $\mathcal{D}^{\text{mech}}\left(\bullet\ ;\ \beta\right)$ where the new unknown model parameter β can be factorized as is the case for classic models with associated evolution equations ($\mathcal{D}^{\text{mech}} = \beta\ \overline{\mathcal{D}}^{\text{mech}}$, see [15]), changes nothing at the intrinsic overparameterization of the heat equation. Only if at least one model parameter is known a priori, or if the model parameter cannot be factorized in at least one addend are all model parameters identifiable, at least in principle.

Since the model at hand uses non-associated evolution equations leading to the plasticity induced heat sources as defined by Equation (2), the general identifiability of all unknown parameters (thermal model parameters as well as boundary coefficients) is therefore given and the question of identifiability posed in the introduction reduces to the question whether or not the temperature field of a simple specimen under mechanical load contains enough information for a locally unique result which will be analyzed by means of a grid search approach.

3.2 | Boundary value problem

The boundary value problem required for the solution of the inverse problem is defined according to the experimental setup and the specimen's geometry. Figure 6 shows the discretization of the specimen which is done by using 3840 brick elements (4 elements in thickness direction) with linear shape functions and by utilizing the underlying symmetry. Homogeneous Dirichlet boundary conditions are applied to the displacement field on the left (green) clamping area. The measured reaction force is applied to the right (blue) clamping surface together with linear displacement constraints, rendering the simulation force controlled. Regarding the boundary conditions of the thermal field, 1280 surface elements govern the heat exchange with the environment according to Equation (3). The specimen can be divided into two parts, one which exchanges heat with the surrounding air and one which exchanges heat with the clamping jaws. Four parameters therefore define the actual thermal boundary conditions, that is, the convection coefficient $\alpha_{\text{con}}^{\text{air}}$ and air temperature θ^{air}, as well as the conduction coefficient $\alpha_{\text{con}}^{\text{cl}}$ and the clamping jaw temperature θ^{cl}. Of these

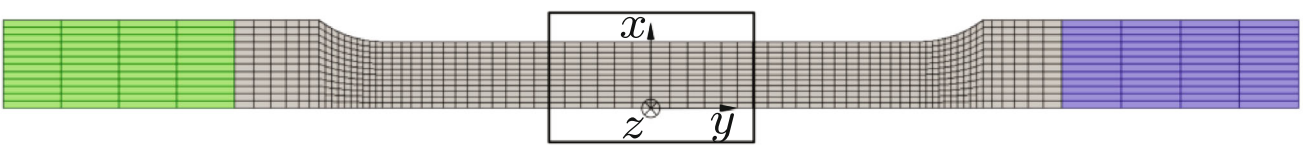

FIGURE 6 Discretized FE model of the specimen. Reprinted from [14], with permission from Elsevier.

four parameters only the temperatures can be measured and prescribed directly, see Table 1. The convection and conduction coefficient depend on various factors (such as material pairing, pressure, airflow, geometry) and are generally unknown.

3.3 | Objective function

In this work, a successive scheme is used following the framework for the identification of material parameters $\boldsymbol{\kappa}$ at low temperature rises for thermo-mechanically coupled material models as presented in [14]. At first, the mechanical material parameters are identified by minimizing the objective function

$$f^{\mathrm{u}} = \sum_{i \in \{x,\, y\}} W_i^{\mathrm{u}} \sum_{t=1}^{n_{\mathrm{ts}}} \left[\Delta \mathbf{u}_i^{\mathrm{exp}} - \Delta \mathbf{u}_i(\boldsymbol{\kappa})\right]_t^2 = \sum_{i \in \{x,\, y\}} W_i^{\mathrm{u}} \sum_{t=1}^{n_{\mathrm{ts}}} \sum_{n=1}^{n_{\mathrm{np}}} \left[\Delta u_{ni}^{\mathrm{exp}} - \Delta u_{ni}(\boldsymbol{\kappa})\right]_t^2 = \sum_{i \in \{x,\, y\}} W_i^{\mathrm{u}} \sum_{t=1}^{n_{\mathrm{ts}}} \sum_{n=1}^{n_{\mathrm{np}}} \left[r_{ni}^{\Delta \mathrm{u}}(\boldsymbol{\kappa})\right]_t^2, \quad (7)$$

which compares relative displacements $\Delta\mathbf{u}$ of simulation and experiment in a least square sense at chosen time steps t. The thermal material parameters as well as the thermal boundary coefficients are identified afterwards, employing the error of the rise in temperature

$$f^{\theta} = W^{\theta} \sum_{t=1}^{n_{\mathrm{ts}}} \left[\Delta \boldsymbol{\theta}^{\mathrm{exp}} - \Delta \boldsymbol{\theta}(\boldsymbol{\kappa})\right]_t^2 = W^{\theta} \sum_{t=1}^{n_{\mathrm{ts}}} \sum_{n=1}^{n_{\mathrm{np}}} \left[\Delta \theta_n^{\mathrm{exp}} - \Delta \theta_n(\boldsymbol{\kappa})\right]_t^2 = W^{\theta} \sum_{t=1}^{n_{\mathrm{ts}}} \sum_{n=1}^{n_{\mathrm{np}}} \left[r_n^{\theta}(\boldsymbol{\kappa})\right]_t^2. \quad (8)$$

For the work at hand, the value of $W^{\theta} = 1$ is chosen. It is worth noting that experimental data is interpolated onto the finite element (FE) nodes in a preprocessing step, and that only the n_{np} FE nodes on the surface of the discretized specimen which are within the black rectangle shown in Figure 6 contribute to the objective function value.

3.4 | Mechanical material parameters

The mechanical parameters are identified in two steps, identifying first the elastic material parameters (Young's modulus E and Poisson's ratio ν) and subsequently the plastic material parameters (initial Yield limit M_{y_0}, nonlinear hardening parameters h and b as well as the one independent yield surface parameter F, see discussion in [14] for details on dependency of specific model parameters for simple tension). The obtained parameter values are summarized in Table 2. Furthermore, Figure 7 shows the resulting fit between simulation and experiment.

3.5 | Reference solution with prescribed boundary coefficients

Before optimizing the thermal boundary coefficients along with the thermal material parameters, a reference solution with prescribed convection and conduction coefficient is generated. The obtained parameters are subsequently compared to the solution based on the, say, full optimization, see Section 3.6.

According to [15], a locally unique fit of the thermal material parameters (i.e., thermal expansion α_{exp}, heat conduction κ_{therm}, heat capacity c_0, and the parameter scaling latent heat, respectively dissipation β) is possible for the specific combination of model and material at hand and yields thermal material parameters close to literature values. In that publication, it was assumed that the boundary coefficients can be prescribed as $\alpha_{\mathrm{con}}^{\mathrm{air}} = 0$ and $\alpha_{\mathrm{con}}^{\mathrm{cl}} = 10^8$ W/(m^2 K) since the heat exchange through the clamping jaws appears to dominate. The optimized thermal material parameters for the experimental data at hand can be found in Table 3. Figure 8 shows the fit of the temperature time relation for a single,

TABLE 2 Optimal values for mechanical material parameters.

Material parameter	E (MPa)	ν	M_{y_0} (MPa)	h (MPa)	b	F
Optimal value	68 396.66	0.34	128.92	1780.65	10.87	0.35

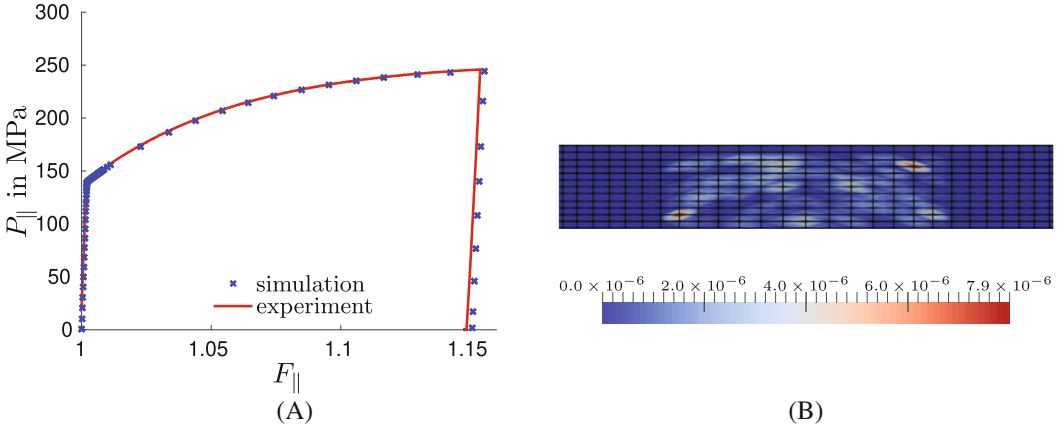

FIGURE 7 Optimized mechanical material parameters lead to a very good agreement between simulation and experiment with respect to displacements and reaction force. (A) Stress–strain relation of experiment and simulation evaluated at midpoint of the specimen. (B) Remaining nodal contribution to the objective function f^{u} (squared error in relative displacements) at time $t = 140$ s

TABLE 3 Obtained reference values for the thermal material parameters and remaining error contribution to the objective function f^{θ}

Material parameter	α_{exp} (10^{-6}/K)	κ_{therm} (mW/mm K)	c_0 (mJ/mm^3 K)	β (–)	$\alpha_{\mathrm{con}}^{\mathrm{air}}$ (W/m^2 K)	$\alpha_{\mathrm{con}}^{\mathrm{cl}}$ (W/m^2 K)	f^{θ} (–)
Optimal value	20.04	175.17	2.35	0.81	0.00	10^8	20.04

Note: Prescribed values are marked in grey.

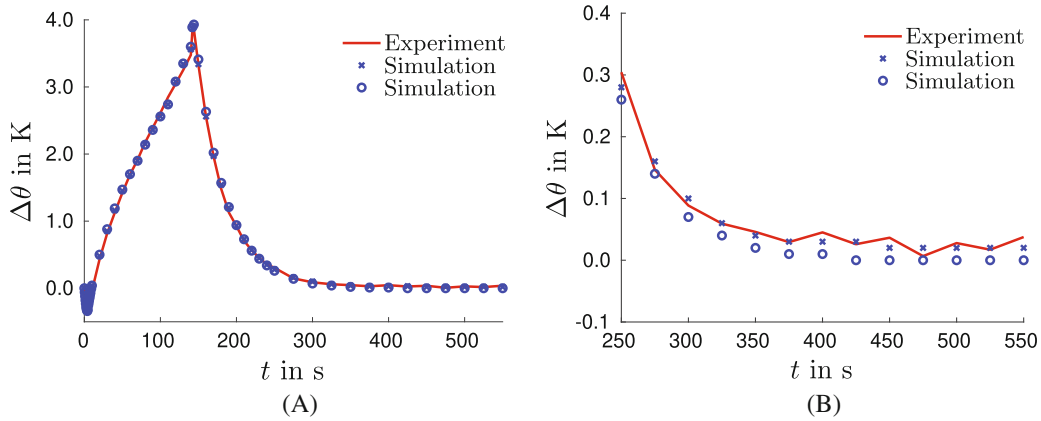

FIGURE 8 Local temperature time relation of experiment and simulations using optimal parameter sets, evaluated at midpoint of the specimen. Identification with prescribed boundary coefficients (∘) from Section 3.5 and identification including boundary coefficients (×). Temperature field is evaluated at midpoint but representative for all nodes considered. (A) Data over the whole time range. (B) Data at the end of the cooling down phase

representative FE node of the specimen. The overall fit of the material response can later be compared against the material response of the fully optimized parameter set, which would be expected to be even better. It is worth noting that this assumption regarding the heat transfer coefficients is only possible due to the high conductivity of the aluminum alloy under consideration and cannot be transferred to other materials in general.

3.6 | Identification of thermal material parameters and boundary coefficients

It was already mentioned in Section 3.2 that the thermal boundary coefficients are generally unknown, so that the set of sought parameters includes the classic thermal material parameters, the material parameter governing dissipation,

TABLE 4 Initial guess for thermal material parameters

Set	α_{exp} (10^{-6} /K)	κ_{therm} (mW/ mm K)	c_0 (mJ/ mm^3 K)	β (–)	α_{con}^{air} (W/ m^2 K)	α_{con}^{cl} (W/ m^2 K)
κ_A	19.83	189.89	2.21	0.81	0.10	$4 \cdot 10^5$
κ_B	23.00	200.00	2.43	1.00	0.10	$4 \cdot 10^5$
κ_C	46.00	200.00	2.43	1.00	0.10	$4 \cdot 10^5$
κ_D	23.00	400.00	2.43	1.00	0.10	$4 \cdot 10^5$
κ_E	23.00	200.00	4.86	1.00	0.10	$4 \cdot 10^5$
κ_F	23.00	200.00	2.43	0.10	0.10	$4 \cdot 10^5$
κ_G	23.00	200.00	2.43	1.00	1.00	$4 \cdot 10^5$
κ_H	23.00	200.00	2.43	1.00	0.10	$8 \cdot 10^5$
κ_I	12.00	400.00	1.22	0.50	0.05	$2 \cdot 10^5$
κ_J	46.00	100.00	4.86	1.00	1.00	$8 \cdot 10^5$

Note: The first set uses values from [15]. The second set uses literature values (as far as they exist). Based on the latter set, one of the parameters was modified in turn by a factor of at least 2 to obtain sets C–H. All parameters are varied to obtain sets I and J.

TABLE 5 Obtained values for the thermal material parameters and remaining error contribution to the objective function f^θ

Set	α_{exp} (10^{-6} /K)	κ_{therm} (mW/ mm K)	c_0 (mJ/ mm^3 K)	β (–)	α_{con}^{air} (W/ m^2 K)	α_{con}^{cl} (W/ m^2 K)	f^θ (–)
κ_A^*	20.21	133.45	2.22	0.79	14.72	236.30	14.97
κ_B^*	20.21	133.41	2.22	0.79	14.73	236.04	14.97
κ_C^*	20.21	133.40	2.21	0.79	14.73	236.10	14.97
κ_D^*	20.20	133.46	2.22	0.79	14.71	236.44	14.97
κ_E^*	20.21	133.43	2.22	0.79	14.72	236.44	14.97
κ_F^*	20.20	133.32	2.21	0.79	14.75	234.92	14.97
κ_G^*	20.21	133.35	2.22	0.79	14.74	236.11	14.97
κ_H^*	20.21	133.41	2.22	0.79	14.73	236.27	14.97
κ_I^*	20.20	133.37	2.22	0.79	14.73	236.46	14.97
κ_J^*	20.21	133.39	2.22	0.79	14.73	236.41	14.97

respectively latent heat, as well as the convection and the conduction coefficient, that is, $\alpha_{\text{con}}^{\text{air}}$ and $\alpha_{\text{con}}^{\text{cl}}$. The identification is started from 10 different initial guesses, see Table 4, to ensure that the experimental data holds the required information to find a locally unique parameter set which minimizes the objective function.

Table 5 shows the obtained values which are identical for all 10 cases. While this may not prove (local) uniqueness in a mathematical sense, it nevertheless suggests that no further minima are to be expected within the vicinity of the obtained solution. Thus, the unknown parameters also appear to be independent in the sense that no direct relation (neither linear nor nonlinear) connects two or more parameters which would lead to an infinite number of solutions.

Remark 1. Further investigations regarding identifiability might involve an analysis of the Hessian of the objective function, as proposed in [4] and applied to the identification of mechanical material parameters in [10]. However, this is usually not done with the true Hessian, the derivation and implementation of which can be rather intricate, but with an approximation based on the Jacobian of the residuum $\boldsymbol{J}_n^{\text{r}} = \frac{\mathrm{d}r_n}{\mathrm{d}\boldsymbol{\kappa}}$. This approximation of the Hessian of the objective function

$$\boldsymbol{H}^{\text{f}} = 2 \sum_{t=1}^{n_{\text{ts}}} \sum_{n=1}^{n_{\text{np}}} W \left[\boldsymbol{J}_n^{\text{r}} \otimes \boldsymbol{J}_n^{\text{r}} + \cancel{r_n \boldsymbol{H}_n^{\text{r}}} \right]_t \tag{9}$$

(exemplarily shown here for $f = f^{\theta}$) is usually associated with the assumption that the second addend in (9) is significantly smaller than the first part. This assumption can, unfortunately, not be examined without computing the neglected addend, generating a conflict between making the assumption in order to avoid derivational and implementational effort and the necessity to prove the validity of the assumption. Alternatively, the absolute value of the residuum $r \ll 1$ close to the optimum is typically considerer in order to discard the second addend. The value of the residuum, however, can simply be scaled, for example, by changing the underlying system of units, and is therefore difficult (maybe even impossible) to interpret. Nevertheless, it is noteworthy that the absolute value for $r_n^{\theta} \sim 10^{-2}$ to 10^{-1} is two orders of magnitudes higher compared to $r_n^{\text{u}} = r_{nx}^{\text{u}} + r_{ny}^{\text{u}} \sim 10^{-4}$ to 10^{-3}, see Figures 7B and 9.

3.6.1 | Comparison with reference solution

So far, it has been shown that the identification of boundary coefficients alongside the thermal material parameters is possible, in principle, on the basis of full field temperature measurements. Comparing the obtained values of such an identification process with the results from the reference solution, which incorporated reasonable values for the boundary coefficients prescribed, shows some significant differences that are worth mentioning.

Subjecting the boundary coefficients to the optimization process allows the remaining squared error value at the end of the optimization f^{θ} to drop by approximately 25% from 20.04 to 14.97, see Tables 3 and 5. The optimal values for the three thermal material parameters α_{exp}, c_0, and β are almost identical and for both cases close to available literature values. Regarding the convection coefficient κ_{therm}, the obtained value lies in the expected range of 2–25 W/(m^2 K) for free convection, see, for example, [11]. There is no expected value for the conduction coefficient, but it is roughly 20 times higher than the convection coefficient, underlining the assumption made in Section 3.5 that heat exchange through the clamping jaws dominates the heat exchange with the environment. The change in boundary coefficients apparently leads to a major difference between the two solutions which lies in the optimal value of the thermal conductivity κ_{therm}. Comparing the material response on the basis of the two parameter sets in Figure 8 shows that both solutions nevertheless

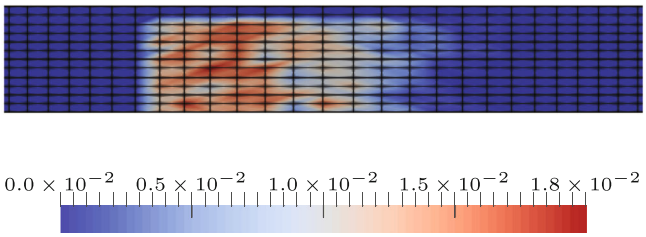

FIGURE 9 Remaining nodal contribution to the objective function f^{θ} (squared error in temperature rise) at time $t = 140$ s

fit the experimental temperature almost equally well. The most notable difference lies in the fit of the end temperature which does not return to the initial temperature (for a node at the center of the specimen), but remains at a slightly higher value. This effect is based on the different temperatures of air and clamping jaws, combined with the plastic deformation of the specimen during mechanical loading. The difference in room- to clamping jaw temperature leads to a higher steady state temperature at the center point for an elongated specimen and can be reproduced by a simulation, only in case heat exchange with the surrounding air is considered. Thus, the temperature rise returns to zero for the parameter set with the prescribed boundary coefficients, since those boundary coefficients were chosen to represent isothermal conditions at the clamping jaws and adiabatic behavior toward air. In contrast thereto, the optimized convection coefficient enables a reasonable amount of heat to be exchanged with the air leading to the aforementioned effect of a slightly higher remaining steady state temperature toward the center of the specimen.

The model is therefore able to represent this behavior by adapting the boundary coefficients but requires a significant change in the thermal conductivity, in order to maintain the overall good match. As discussed above, the effect of the remaining steady state temperature depends on the temperature difference between air and clamping device. Those values are prescribed in the simulation and rely on a measurement that is, like all measurements, subject to measurement errors. Thus, the question of sensitivities toward measured boundary temperatures arises, as addressed in the following.

3.6.2 | Sensitivity investigations

Thermal material parameters and boundary coefficients are identified again, but with modified boundary temperatures in the simulation. Prescribed values as well as resulting optimal model parameters are summarized in Tables 6 and 7. The precise temperature value of either air or clamping jaws does not matter as much as the actual difference, for results are almost identical as long as the prescribed temperature difference is also identical. Thus, the values from Table 6 are visualized in Figure 10, showing the relative change of optimal values with respect to the prescribed temperature difference between air and clamping jaws.

Figure 10A,B shows that reasonable measurement errors in the prescribed external temperature difference have very little effect on the optimal value for the thermal expansion coefficient α_{exp}, the heat capacity c_0 and the scaling parameter β, which only change up to 4% for the case at hand. In contrast thereto, the optimal values of the remaining material parameter κ_{therm} as well as the unknown boundary coefficients react very sensitively to a change of the prescribed temperature difference and may differ up to 60%. Furthermore, the overall trend indicates the intrinsic correlation of the three latter parameters, all of which define a different type of heat conductivity. A drastic change in one (conductivity)

TABLE 6 Obtained values for the thermal material parameters and remaining error contribution to the objective function f^{θ} with modified air temperature in the simulation

$\Delta\theta$ (K)	θ^{air} (K)	θ^{cl} (K)	α_{exp} (10^{-6}/K)	κ_{therm} (mW/mm K)	c_0 (mJ/mm^3 K)	β (–)	$\alpha_{\text{con}}^{\text{air}}$ (W/m^2 K)	$\alpha_{\text{con}}^{\text{cl}}$ (W/m^2 K)	f^{θ} (–)
0.00	296.70	296.70	20.01	154.32	2.19	0.79	11.99	183.16	16.87
0.10	296.80	296.70	20.11	144.84	2.20	0.79	13.35	182.76	16.52
0.30	297.00	296.70	20.19	136.80	2.21	0.79	14.41	197.83	15.88
0.50	297.20	296.70	20.23	133.11	2.22	0.79	14.85	217.62	15.35
0.60	297.30	296.70	20.21	133.43	2.22	0.79	14.75	227.67	15.14
0.70	297.40	296.70	20.21	133.45	2.22	0.79	14.72	236.30	14.97
0.80	297.50	296.70	20.20	133.63	2.21	0.79	14.66	244.89	14.84
0.90	297.60	296.70	20.15	137.06	2.21	0.78	14.13	250.65	14.74
1.10	297.80	296.70	20.03	146.58	2.20	0.78	12.63	264.28	14.65
1.30	298.00	296.70	19.88	159.85	2.19	0.78	10.54	278.13	14.65
1.80	298.50	296.70	19.66	183.17	2.17	0.77	6.99	300.49	14.71
2.30	299.00	296.70	19.55	194.77	2.16	0.77	5.08	311.27	14.76

Note: Variation increases with distance to measured temperature values in Table 1. Prescribed values marked in grey.

TABLE 7 Obtained values for the thermal material parameters and remaining error contribution to the objective function f^θ with modified clamping temperature in the simulation

$\Delta\theta$ (K)	θ^{air} (K)	θ^{cl} (K)	α_{exp} (10^{-6}/K)	κ_{therm} (mW/mm K)	c_0 (mJ/mm^3 K)	β (–)	$\alpha^{\text{air}}_{\text{con}}$ (W/m^2 K)	$\alpha^{\text{cl}}_{\text{con}}$ (W/m^2 K)	f^θ (–)
0.10	297.40	297.30	20.07	144.83	2.20	0.79	13.35	182.78	16.52
0.30	297.40	297.10	20.17	136.91	2.21	0.79	14.40	197.50	15.88
0.50	297.40	296.90	20.21	133.48	2.22	0.79	14.79	217.69	15.35
0.60	297.40	296.80	20.21	133.59	2.22	0.79	14.73	227.86	15.14
0.70	297.40	296.70	20.21	133.45	2.22	0.79	14.72	236.30	14.97
0.80	297.40	296.60	20.20	133.43	2.21	0.79	14.70	244.26	14.84
0.90	297.40	296.50	20.16	137.06	2.21	0.78	14.13	250.65	14.74
1.10	297.40	296.30	20.06	146.53	2.20	0.78	12.64	264.03	14.65

Note: Variation increases with distance to measured temperature values in Table 1. Prescribed values marked in grey.

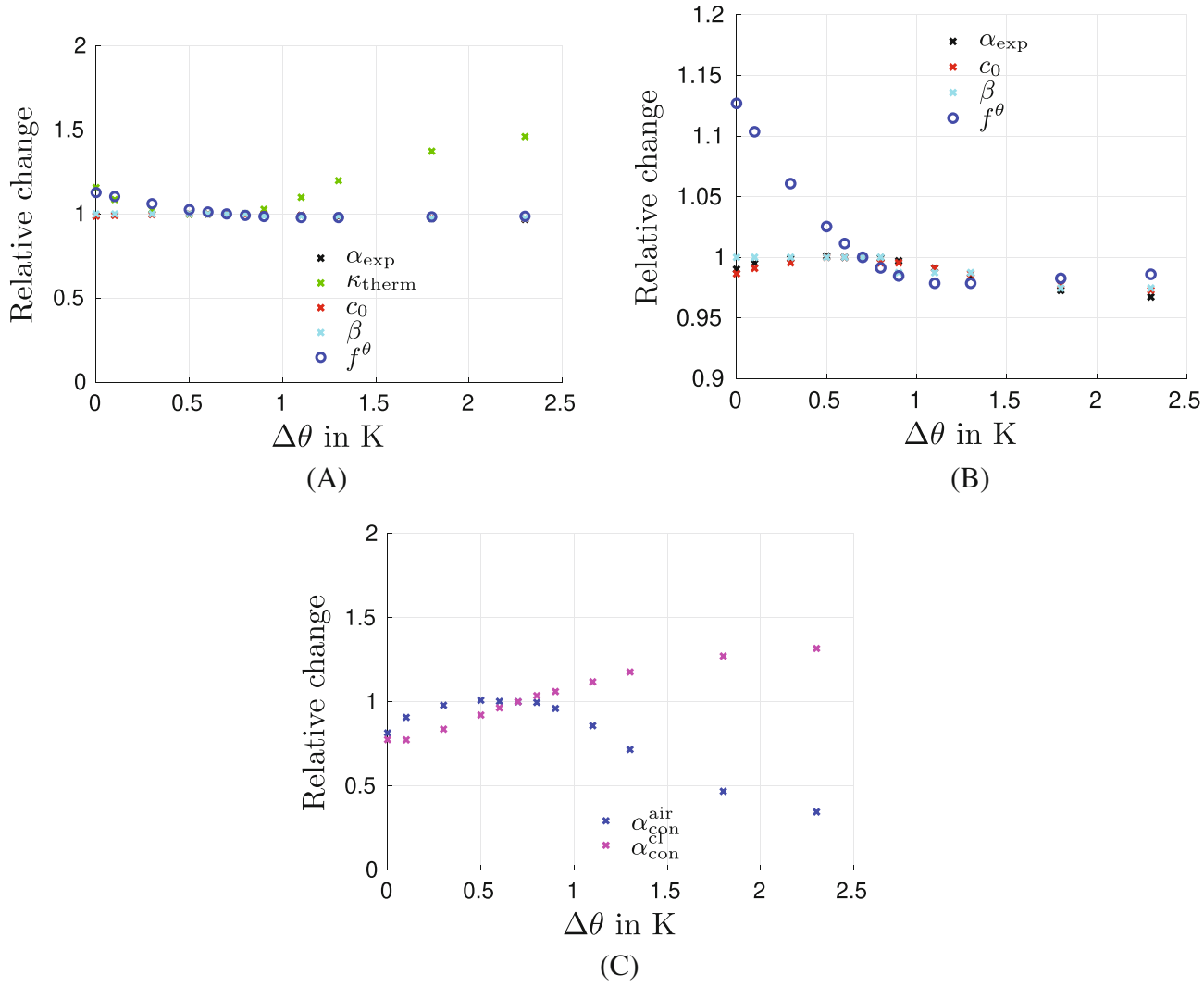

FIGURE 10 Relative change of model parameter with respect to prescribed temperature difference of air and clamping jaws ($\theta^{\text{air}} - \theta^{\text{cl}}$). References are the values corresponding to the measured temperature difference of 0.7 K. (A) Sensitivity of thermal material parameters and remaining squared error. (B) Zoom to parameters with low sensitivity. (C) Sensitivity of thermal boundary coefficients

parameter necessitates the other two parameters to change accordingly, in order to maintain the overall temperature fit. It is worth mentioning that, although the correlation between the parameters κ_{therm}, $\alpha_{\text{con}}^{\text{air}}$, and $\alpha_{\text{con}}^{\text{cl}}$ may be high, it is not a perfect correlation in the sense of dependency (linear or nonlinear), which would have led to multiple equally suitable solutions in Section 3.6. Thus, an identification of thermal boundary coefficients for low temperature rises appears possible but requires a precise measurement of temperatures at the surfaces of the specimen. Alternatively, an experimental setup which guarantees an identical temperature of air and testing machine would circumvent the problem of this kind of sensitivity, since the identification is not as sensitive to the overall temperature level as it is to a difference in prescribed temperatures at the boundaries.

3.7 | Identification with reduced set of unknowns

There may be applications where the classic thermal material parameters can either be preidentified by using specialized experiments or simply be taken from literature. For those cases, the identification process reduces to the optimization of the scaling parameter β and of the thermal boundary coefficients. Table 8 shows the result of such an identification for the aluminum alloy at hand. It can be seen that the remaining error value increases by 17% when compared to the solution with prescribed boundary coefficients and increases by 58% when compared to the solution with the optimized boundary coefficients. However, the obtained values are still within reasonable bounds. Moreover, this immense (relative) increase in remaining error can be put into perspective if the actual material response of the three parameter sets (Tables 3, 5, and 8) is compared with the experimental data. Figure 11 reveals an almost insignificant absolute difference between the material response of the three parameter sets mentioned before. This is due to the specific material model chosen which can adapt the remaining thermal material parameter β to obtain a slightly less optimal, but nevertheless still respectable, fit to the experimental data. Depending on the overall model formulation, it is therefore possible to either optimize the thermal

TABLE 8 Obtained values for the model parameters and remaining error contribution to the objective function f^{θ} using available literature values

Material parameter	α_{exp} (10^{-6}/K)	κ_{therm} (mW/mm K)	c_0 (mJ/mm^3 K)	β (–)	$\alpha_{\text{con}}^{\text{air}}$ (W/m^2 K)	$\alpha_{\text{con}}^{\text{cl}}$ (W/m^2 K)	f^{θ} (–)
Optimal value	23.00	200.00	2.43	0.93	2.18	976.00	23.59

Note: Prescribed values are marked in grey.

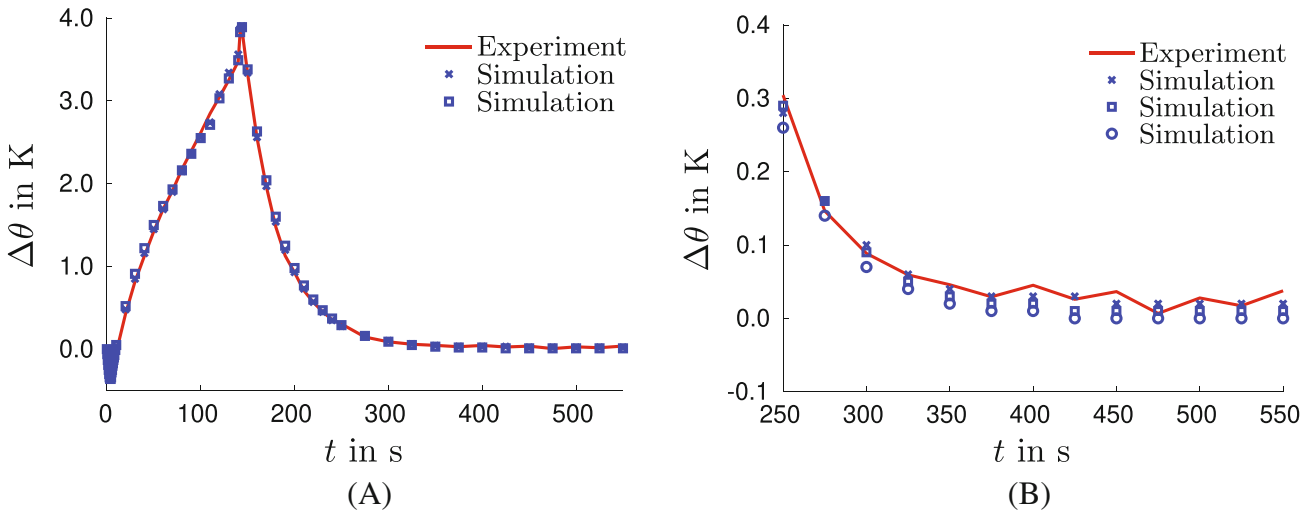

FIGURE 11 Local temperature time relation of experiment and simulations using optimal parameter sets, evaluated at midpoint of the specimen. Identification with prescribed boundary coefficients (∘) from Section 3.5, identification with whole set of optimized model parameters (×) from Section 3.6, and identification with prescribed thermal material parameters (□). Temperature field is evaluated at midpoint but representative for all nodes considered. (A) Data over the whole time range. (B) Data at the end of the cooling-down phase

material parameters along with the thermal boundary coefficients or to prescribe some parameter values (which were identified by means of other boundary value problems, e.g., simple heat conductor) while still maintaining a satisfyingly precise fit.

4 | CONCLUSIONS

This work focuses on the identification of coefficients related to Robin-type boundary conditions together with thermal material parameters and answers the questions of identifiability, (local) uniqueness, and sensitivity in an empirical manner. The identification is based on full field temperature measurements and uses surface elements which require a (generally unknown) convection, respectively conduction coefficient and the temperature of the surrounding medium. The latter one is measurable and was found to be non-equal for air and clamping jaws during the experiment at hand.

Identifications starting from several initial guesses all converge toward the same optimum, suggesting that the solution is unique within a certain (trust) area. Based on this, it directly follows that the unknown parameters are independent and not connected via some linear or non-linear relation which would otherwise lead to a valley of solutions. Comparing the obtained parameters with a reference solution based on reasonable, prescribed values for the boundary coefficients already indicates a higher correlation between heat conduction and the two boundary coefficients, that is, κ_{therm}, $\alpha_{\text{con}}^{\text{air}}$, and $\alpha_{\text{con}}^{\text{cl}}$, respectively. Not only does an analysis using different prescribed temperature differences for the surrounding air and clamping jaws underline the correlation of the three conduction-like model parameters, it furthermore shows the sensitivity of the optimal values with respect to small changes in the prescribed temperature difference of the surrounding media. To be more precise, a different prescribed external temperature difference naturally leads to different optimal values for the heat conduction and heat convection coefficient. These two parameters are very sensitive to the aforementioned changes and, moreover, cause an equally severe sensitivity in the thermal conduction coefficient due to the high correlation between the three parameters. Thus, the optimal value of the thermal conduction coefficient changes drastically with the prescribed temperature difference and is therefore extremely dependent on measurement errors. The temperature field may therefore hold enough information to allow a simultaneous identification of thermal material parameters and boundary coefficients, but requires a precise measurement of external surrounding temperatures to obtain meaningful results.

It is worth mentioning that meaningful and optimal parameters are not necessarily the same as valid model parameters which could be used to describe other boundary value problems (e.g., simple heat conductor) equally well. It was already shown in [15] that optimal model parameter values for thermo-mechanically coupled material models depend on the model formulation (e.g., on the model-specific prediction of dissipated energy). Thus, if thermal material parameters are identified a priori by means of specialized experiments or taken from literature, the optimization of the remaining model parameters yields different parameter values and the obtained fit to experimental temperature data may worsen (by almost 60% for the case at hand), but the actual absolute error may remain within reasonable limits (depending on the adaptability of the model).

Using this work as a basis, it is now possible to apply the underlying identification framework to materials which undergo a higher temperature rise during loading in order to see whether this reduces the sensitivity toward external temperatures rendering the whole process closer to practical applications. However, this may involve more complex material behavior, respectively models, such as viscous response and damage effects which contribute to dissipation and therefore plastic heating. Modeling these effects will likely introduce further sources of discrepancy between actual and predicted dissipation, so that an identification, that is, optimization, for such a pairing of material and model is nontrivial and highly model dependent.

CONFLICT OF INTEREST

The authors declare no potential conflict of interests.

ACKNOWLEDGEMENTS

Open Access funding enabled and organized by Projekt DEAL.

REFERENCES

[1] W. P. Adamczyk, T. Kruczek, G. Moskal, and R. A. Białecki, Nondestructive technique of measuring heat conductivity of thermal barrier coatings, Int. J. Heat Mass Transf. **111** (2017), 442–450.
[2] A. Bartels, T. Bartel, M. Canadija, and J. Mosler, On the thermomechanical coupling in dissipative materials: A variational approach for generalized standard materials, J. Mech. Phys. Solids **82** (2015), 218–234.
[3] J. Beck and A. Osman, Nonlinear inverse problem for the estimation of time-and-space-dependent heat-transfer coefficients, J. Thermophys. Heat Transf. **3** (1989), 146–152.
[4] J. V. Beck and K. J. Arnold, *Parameter estimation in engineering and science*, Wiley, Hoboken, NJ, 1977.
[5] E. Berkovich, A. Golubeva, E. Shadek, and L. Tukh, Use of methods of solving inverse problems of heat conduction to establish the coefficient of heat transfer in jet cooling, J. Eng. Phy **34** (1978), 619–624.
[6] S. Chantasiriwan, Inverse determination of steady-state heat transfer coefficient, Int. Commun. Heat Mass Transf. **27** (2000), 1155–1164.
[7] F. Chunli, S. Fengrui, and Y. Li, A numerical method on inverse determination of heat transfer coefficient based on thermographic temperature measurement, Chinese J. Chem. Eng. **16** (2008), 901–908.
[8] P. Du, G. Wang, Z. Nie, and Y. Rong. *A FEM-based inverse calculation method for determination of heat transfer coefficient in liquid quenching process*, Proc. 143rd Annu. Meet. Exhib., TMS 2014, San Diego, California, 2014, pp. 309–315.
[9] L. Fiala, M. Jerman, P. Reiterman, and R. Černý, Determination of thermal conductivity of silicate matrix for applications in effective media theory, Int. J. Thermophys. **39** (2018), 28.
[10] S. Hartmann and R. R. Gilbert, Identifiability of material parameters in solid mechanics, Arch. Appl. Mech. **88** (2018), 3–26.
[11] F. P. Incropera, A. S. Lavine, T. L. Bergman, and D. P. DeWitt, *Fundamentals of heat and mass transfer*, Wiley, Hoboken, NJ, 2007.
[12] R. Mahnken, An inverse finite-element algorithm for parameter identification of thermoelastic damage models, Int. J. Numer. Methods Eng. **48** (2000), 1015–1036.
[13] W. Parker, R. Jenkins, C. Butler, and G. Abbott, Flash method of determining thermal diffusivity, heat capacity, and thermal conductivity, J. Appl. Phy. **32** (1961), 1679–1684.
[14] L. Rose and A. Menzel, Optimisation based material parameter identification using full field displacement and temperature measurements, Mech. Mater. **145** (2020), 103292.
[15] L. Rose and A. Menzel, Identification of thermal material parameters for thermo-mechanically coupled material models, Meccanica **56** (2021), 393–416.

How to cite this article: L. Rose, and A. Menzel, *On the determination of thermal boundary conditions for parameter identifications of thermo-mechanically coupled material models*, GAMM-Mitteilungen. **45** (2022), e202200010. https://doi.org/10.1002/gamm.202200010

APPENDIX A. MODEL EQUATIONS

All model equations are summarized in this section. A detailed derivation of this model can be found in [15].

Helmholtz free energy

$$\psi = \psi^{\mathrm{el}} + \psi^{\mathrm{pl}} + \psi^{\mathrm{ther}} + \psi^{\mathrm{coup}} + \psi^{\mathrm{ns}}, \quad \text{with} \tag{A1}$$

$$\psi^{\mathrm{el}} = \frac{\lambda}{2} \ln^2(J^{\mathrm{el}}) + \frac{\mu}{2} \left[\mathrm{tr}(\boldsymbol{C}^{\mathrm{el}}) - 3\right] - \mu \ln(J^{\mathrm{el}}), \tag{A2}$$

$$\psi^{\mathrm{pl}} = \frac{1}{2} h\, \alpha^2, \tag{A3}$$

$$\psi^{\mathrm{ther}} = c_0 \left[\theta - \theta_0 - \theta \ln\left(\frac{\theta}{\theta_0}\right)\right], \tag{A4}$$

$$\psi^{\mathrm{coup}} = -3\, \alpha_{\mathrm{exp}}\, K_{\mathrm{bulk}}\, [\theta - \theta_0] \frac{\ln(J^{\mathrm{el}})}{J^{\mathrm{el}}}, \tag{A5}$$

$$\psi^{\mathrm{ns}} = [1 - \beta]\, M_{y_0}\, \alpha. \tag{A6}$$

Kinematics and driving forces

$$\boldsymbol{F} = \boldsymbol{F}^{\mathrm{el}} \cdot \boldsymbol{F}^{\mathrm{pl}}, \tag{A7}$$

$$\boldsymbol{P} = \frac{\partial \psi}{\partial \boldsymbol{F}^{\mathrm{el}}} \cdot \left[\boldsymbol{F}^{\mathrm{pl}}\right]^{-\mathrm{t}}, \tag{A8}$$

$$\boldsymbol{M} = \left[\boldsymbol{F}^{\mathrm{el}}\right]^{\mathrm{t}} \cdot \boldsymbol{P} \cdot \left[\boldsymbol{F}^{\mathrm{pl}}\right]^{\mathrm{t}} = \left[\boldsymbol{F}^{\mathrm{el}}\right]^{\mathrm{t}} \cdot \frac{\partial \psi}{\partial \boldsymbol{F}^{\mathrm{el}}}, \tag{A9}$$

$$K = -\frac{\partial \psi}{\partial \alpha}, \tag{A10}$$

$$\overline{K} = -\frac{\partial \psi^{\mathrm{pl}}}{\partial \alpha}, \tag{A11}$$

$$\boldsymbol{q} = -\kappa_{\mathrm{therm}} \, \nabla_{\boldsymbol{x}} \theta. \tag{A12}$$

Yield surface

$$\begin{aligned} \Phi &= \sqrt{\boldsymbol{M} : \mathbf{G} : \boldsymbol{M}} - \beta \, M_{y_0} + K \\ &= \sqrt{\boldsymbol{M} : \mathbf{G} : \boldsymbol{M}} - M_{y_0} + \overline{K} \\ &= \left[F[M_{11} - M_{22}]^2 + G[M_{33} - M_{11}]^2 + H[M_{22} - M_{33}]^2 + 2\,L\,M_{12}^2 + 2\,M\,M_{23}^2 + 2\,N\,M_{13}^2\right]^{\frac{1}{2}} - M_{y_0} + \overline{K}. \end{aligned} \tag{A13}$$

Plastic potential and evolution equations

$$g = \Phi + \frac{1}{2}\frac{b}{h}\,\overline{K}^2, \tag{A14}$$

$$\boldsymbol{L}^{\mathrm{pl}} = \lambda_{\mathrm{pm}} \, \frac{\partial g}{\partial \boldsymbol{M}}, \tag{A15}$$

$$\dot{\alpha} = \lambda_{\mathrm{pm}} \, \frac{\partial g}{\partial \overline{K}}. \tag{A16}$$

Surface elements

$$q_0 = \boldsymbol{n} \cdot \boldsymbol{q} = -\alpha_{\mathrm{con}} \, \left[\theta^{\mathrm{M}} - \theta\right]. \tag{A17}$$

Time integration

$$(\bullet)_{n+1} = (\bullet)_n + \Delta t \, (\dot{\bullet})_{n+1}. \tag{A18}$$

Energies are defined by using the two Lamé parameters $\lambda = E\,\nu/\left[[1+\nu]\,[1-2\,\nu]\right]$, $\mu = E/\left[2+2\,\nu\right]$ and the bulk modulus $K_{\mathrm{bulk}} = E/\left[3-6\,\nu\right]$, whereas the identification is performed with respect to Young's modulus E and Poisson's ratio ν.